Enhanced cytarabine-induced killing in OGG1-deficient acute myeloid leukemia cells

Nichole Owen[a,1], Irina G. Minko[a], Samantha A. Moellmer[a], Sydney K. Cammann[a], R. Stephen Lloyd[a,b], and Amanda K. McCullough[a,b,2]

[a]Oregon Institute of Occupational Health Sciences, Oregon Health & Science University, Portland, OR 97239; and [b]Department of Molecular and Medical Genetics, Oregon Health & Science University, Portland, OR 97239

Edited by Michael E. O'Donnell, Rockefeller University, New York, NY, and approved January 5, 2021 (received for review August 7, 2020)

Human clinical trials suggest that inhibition of enzymes in the DNA base excision repair (BER) pathway, such as PARP1 and APE1, can be useful in anticancer strategies when combined with certain DNA-damaging agents or tumor-specific genetic deficiencies. There is also evidence suggesting that inhibition of the BER enzyme 8-oxoguanine DNA glycosylase-1 (OGG1), which initiates repair of 8-oxo-7,8-dihydro-2′-deoxyguanosine (8-oxo-dG) and 2,6-diamino-4-hydroxy-5-formamidopyrimidine (Fapy-dG), could be useful in treating certain cancers. Specifically, in acute myeloid leukemia (AML), both the RUNX1-RUNX1T1 fusion and the CBFB-MYH11 subtypes have lower levels of *OGG1* expression, which correlate with increased therapeutic-induced cell cytotoxicity and good prognosis for improved, relapse-free survival compared with other AML patients. Here we present data demonstrating that AML cell lines deficient in OGG1 have enhanced sensitivity to cytarabine (cytosine arabinoside [Ara-C]) relative to OGG1-proficient cells. This enhanced cytotoxicity correlated with endogenous oxidatively-induced DNA damage and Ara-C–induced DNA strand breaks, with a large proportion of these breaks occurring at common fragile sites. This lethality was highly specific for Ara-C treatment of AML cells deficient in OGG1, with no other replication stress-inducing agents showing a correlation between cell killing and low OGG1 levels. The mechanism for this preferential toxicity was addressed using in vitro replication assays in which DNA polymerase δ was shown to insert Ara-C opposite 8-oxo-dG, resulting in termination of DNA synthesis. Overall, these data suggest that incorporation of Ara-C opposite unrepaired 8-oxo-dG may be the fundamental mechanism conferring selective toxicity and therapeutic effectiveness in OGG1-deficient AML cells.

DNA repair | DNA replication | fragile site | DNA polymerase delta | AML therapy

Each year, there are ∼21,000 new cases of acute myeloid leukemia (AML) diagnosed in the United States, with nearly 11,000 AML-associated deaths (1). Based on published data and statistics collected through the National Cancer Institute, survivorship for newly diagnosed AML patients has slowly improved over the past 5 decades with a current 5-y survivorship of ∼28% (1, 2). These data highlight the critical need to identify and validate new targets for AML therapeutics. AML is a heterogeneous disease that exhibits different gene mutations or chromosomal alterations, which define specific AML subtypes. Although the genetic basis underlying AML varies, most patients with newly diagnosed AML are treated uniformly, with a combination of cytarabine (cytosine arabinoside [Ara-C]) and an anthracycline (either daunorubicin or idarubicin) as the standard of care. The standard protocol, 7+3 therapy, involves 7 d of Ara-C and 3 d of anthracycline. Ara-C is a nucleoside analog that functions as an inhibitor of DNA replication, thereby inducing replication stress and associated subsequent cellular dysfunctions (3, 4). Daunorubicin and idarubicin are inhibitors of DNA type II topoisomerases and may also have additional functions in DNA adduct formation (5).

Given the poor responsiveness of most AML subtypes, gene-specific targeted therapies have been developed and have progressed through various stages of clinical trials. One such therapeutic strategy targets patients with activating mutations in the FMS-like tyrosine kinase 3 (FLT3). Specifically, midostaurin, a multikinase inhibitor, and gilteritinib, a more FLT3-selective agent, are approved for treatment of patients with FLT3 mutations (reviewed in refs. 6–8). There are also advanced clinical investigations using the second-generation FLT3-specific inhibitors quizartinib and crenolanib (reviewed in refs. 6, 7). In addition, inhibitors have been developed for two mutated isoforms of isocitrate dehydrogenase (IDH1 or IDH2), ivosidenib (IDH1-specific) and enasidenib (IDH2-specific) (9, 10). The therapeutic efficacy of an inhibitor of the B cell lymphoma (BCL)-2 protein venetoclax has also been demonstrated (11–13). Other potential targets for AML therapeutics include proteins involved in epigenetic control of gene expression, such as the histone methyltransferase DOT1L, the demethylase LSD1, and the MLL-interacting protein menin (reviewed in refs. 14–16).

Limitations of these targeted therapies include the restricted scope of AML patients who would derive benefit from protein-specific drugs and the development of resistance and relapse. For patients treated with 7+3 therapy, the overall prognosis and anticipated lifespan vary greatly, with patients with the RUNX1-RUNX1T1 and CBFB-MYH11 subtypes having an excellent 5-y

Significance

Acute myeloid leukemia (AML) patients whose cancers are classified as either the RUNX1-RUNX1T1 fusion subtype or the CBFB-MYH11 fusion subtype share the common characteristic of significantly decreased levels of mRNA transcripts encoding the DNA repair enzyme *OGG1*. While these two subtypes consistently correlate with the best prognosis for improved relapse-free and overall survival, the molecular basis for relating enhanced survival to low OGG1 has not been established. To identify the basis for this subtype-specific therapeutic efficacy, we demonstrate the mechanism through which the unique combination of the diminution in OGG1 activity and cytarabine treatment confers preferential cell killing, thereby identifying OGG1 as a novel therapeutic target for AML patients with normal or increased levels of OGG1.

Author contributions: N.O., I.G.M., R.S.L., and A.K.M. designed research; N.O., I.G.M., S.A.M., and S.K.C. performed research; N.O., I.G.M., S.A.M., S.K.C., R.S.L., and A.K.M. analyzed data; and N.O., I.G.M., S.A.M., S.K.C., R.S.L., and A.K.M. wrote the paper.

The authors declare no competing interest.

This article is a PNAS Direct Submission.

[1]Present address: Department of Molecular and Human Genetics, Baylor College of Medicine, Houston, TX 77030.

[2]To whom correspondence may be addressed. Email: mcculloa@ohsu.edu.

This article contains supporting information online at https://www.pnas.org/lookup/suppl/doi:10.1073/pnas.2016833118/-/DCSupplemental.

Published March 8, 2021.

overall prognosis (17). Thus, developing a fundamental understanding of the genes and pathways that are differentially affected in these "good prognosis" subtypes may provide insight into strategies to treat the remainder of patients.

To identify genes that are dysregulated in the RUNX1-RUNX1T1 and CBFB-MYH11 subtypes, a key prior investigation showed that the levels of transcripts for the DNA repair enzyme 8-oxoguanine glycosylase-1 (OGG1) were significantly reduced in these cancers, implicating it as a novel prognostic indicator for AML responsiveness (18). OGG1 is an initiator of the DNA base excision repair (BER) pathway and specifically incises DNA at 8-oxo-7,8-dihydro-2′-deoxyguanosine (8-oxo-dG) and 2,6-diamino-4-hydroxy-5-formamidopyrimidine (Fapy-dG) lesions (reviewed in ref. 19). It is the only DNA glycosylase to initiate repair of 8-oxo-dG. Down-regulation of OGG1 has been reported in two cell culture models in which the RUNX1-RUNX1T1 fusion was expressed, $CD34^+$ cord blood (20) and U937 cells (21). Furthermore, the AML cell line KG-1 expresses a biallelic, temperature-sensitive R229Q OGG1 (tsOGG1), which exhibits increased cytotoxicity following incorporation of 8-oxo-dG into DNA (22, 23). The literature also suggests that OGG1 status may affect cellular responses to anticancer treatments, in that suppression of OGG1 via siRNA led to increased sensitivity of cells to antimetabolites, including methotrexate, raltitrexed, and 5-fluorodeoxyuridine (24). Additional previous work showed that three leukemia cell lines with mutated OGG1 or low OGG1 levels were hypersensitive to radiation (25).

Given the significant literature that associates deficiencies in OGG1-initiated repair with positive prognostic indicators in AML and other diseases, this investigation was designed to establish a mechanistic link between the levels of OGG1 activity and chemotherapeutic responsiveness of specific AML subtypes and thus validate OGG1 as a novel target for cancer therapeutics.

Results

Low Levels of *OGG1* messenger RNA Uniquely Correlate with RUNX1-RUNX1T1 AML Subtype. Previous investigations have proposed that decreased levels of *OGG1* messenger RNA (mRNA) commonly observed for RUNX1-RUNX1T1 and CBFB-MYH11 subtypes are a prognostic indicator of AML therapeutic responsiveness (18). Our analyses of The Cancer Genome Atlas (TCGA) (26) compared relative *OGG1* expression across different cytogenetic subtypes of AML and also demonstrated that patient samples of these subtypes have low-level expression of *OGG1* relative to any of the other subtypes (Fig. 1*A*). Because all these patients have AML, these samples represent the same hematopoietic cell lineage, and thus any consistent differences in gene expression are likely related to underlying mutations or translocations within each subtype. Since the major mechanisms of action of both Ara-C and anthracyclines are DNA replication stress and DNA adduct formation, we hypothesized that additional potential candidate genes that could increase the sensitivity to DNA damaging agents may be associated with dysregulation of DNA replication, repair, recombination, and cell cycle regulation. Thus, using the TCGA database of AML samples, we queried an additional 404 genes for correlation between expression levels and AML cytogenetic subtype. These genes included the 318 DNA damage response genes previously reported in our siRNA screen for formaldehyde response (27) and 87 additional genes related to DNA replication, cell cycle, apoptosis, and Ara-C import and metabolism (*SI Appendix*, Table S1). Strikingly, no other gene in our query demonstrated any significant differences in expression as a function of AML subtype, suggesting a potentially unique role for OGG1 in modulating responsiveness of AML cells to chemotherapy.

In addition to our analyses of the TCGA database, we also investigated whether the reduced *OGG1* mRNA levels could be detected in patient cell samples from the Oregon Health & Science University (OHSU) Beat AML cohort (Fig. 1*B*) (28). Analyses of this dataset in Vizome revealed that the median *OGG1* expression levels were lower in the RUNX1-RUNX1T1 and CBFB-MYH11 samples relative to other subtypes and healthy controls.

Transcripts for *OGG1* are differentially spliced to yield both nuclear- and mitochondrial-targeted forms of the enzyme, with isoform 1A the predominant nuclear isoform (29). Since the TCGA and Vizome data captured multiple *OGG1* splice variants, we designed isoform-specific DNA primers to assess the relative abundance of these splice variants in a subset of the Beat AML patient samples and selected cell lines representing several AML subtypes (*SI Appendix*, Table S2). Specifically, primers that quantify isoform 1A versus isoform 1B and other alternatively spliced isoforms were used (Fig. 1*C*), with the left panel showing the relative amount of PCR products generated from a forward primer located within *OGG1* exon 6 and a reverse primer that spanned the junction of exons 6 and 7 that is unique to isoform 1A. The center and right panels show data derived from patient samples for isoforms 1A (spliced) and 1B (intron retained), respectively. Subsets of samples were chosen, including all Beat AML patient samples with a confirmed RUNX1-RUNX1T1 translocation [*t*(8, 21)] and cross-sections of "control" patient samples representing other AML subtypes including MLL rearrangements, inv(3)(q21q26.2) (GATA2-MECOM), NPM1 mutations, *t*(15,17) (PML-RARA), and those with normal karyotypes (Fig. 1*C*). Patient samples harboring the common inv (16) (CBFB-MYH11) were excluded from these analyses, since CBFB and RUNX1 are binding partners in the core binding factor transcription complex, and these patients would not represent a proper control group for this study. One RUNX1-RUNX1T1 patient had several samples available from multiple specimen collections over time (*SI Appendix*, Table S2, blue shading). These samples were used as a control to assess for reproducibility of the data using biological replicates. These analyses revealed that the RUNX1-RUNX1T1 patient samples showed a specific reduction in *OGG1* isoform 1A versus control AML subtypes. Within the RUNX1-RUNX1T1 subtype, the isoform 1A expression levels closely correlated with *OGG1* levels in the same patient sample reported in the Vizome database (vizome.org/aml/), indicating that the overall loss of *OGG1* is likely driven by the loss of *OGG1-1A*. Although samples used in the TCGA dataset are not available for comparable analyses, we infer that decreased levels of isoform 1A likely account for the low-level expression in RUNX1-RUNX1T1 TCGA patient samples.

To conduct mechanistic studies regarding the potential relationship between levels of *OGG1* and chemotherapeutic responsiveness, it was necessary to determine whether AML cell lines also displayed the isoform 1A-specific profile. Thus, isoform-specific PCR analyses were carried out for AML cell lines harboring RUNX1-RUNX1T1 translocations (Kasumi-1 and SKNO-1), wild-type *OGG1* (MOLM-14), and cells harboring a biallelic R229Q inactivating *OGG1* mutation (KG-1). These analyses revealed a specific decrease in the expression level of isoform 1A, but not of isoform 1B, in the Kasumi-1 and SKNO-1 cells (Fig. 1*D*) validating the choice of these cell lines in ongoing mechanistic experimental designs. The KG-1 cells showed no reduction in isoform 1A relative to control MOLM-14 cells. This result was anticipated, since the OGG1 deficiency in KG-1 is known to be the result of protein inactivation under the physiological temperature conditions and not decreased expression levels (30).

RUNX1-RUNX1T1 AML Cells Have Reduced Capacity to Repair Nuclear 8-oxo-dG. Based on the transcription profile data, we hypothesized that reduced levels of mRNA encoding nuclear-targeted OGG1 (isoform 1A) would result in less efficient repair of 8-oxo-dG in the nuclear compartment and increased steady-state

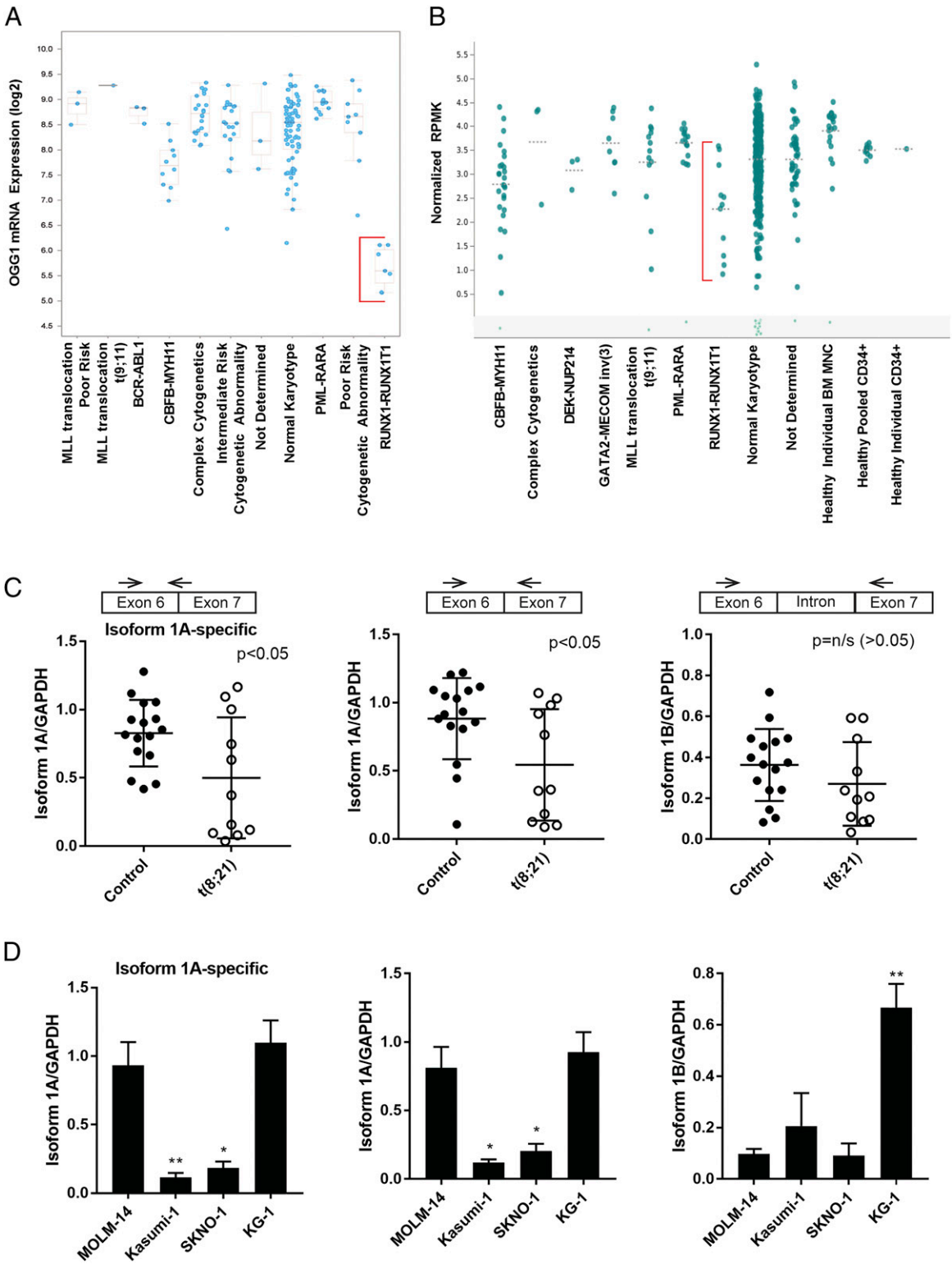

Fig. 1. *OGG1* expression as a function of AML cytogenetic subtype. (*A*) Relative levels of *OGG1* transcript in cytogenetic subtype-specific AML patient samples from the TCGA database. (*B*) Relative levels of *OGG1* transcript in subtype-specific AML patient samples from the Beat AML Vizome database. The red brackets in *A* and *B* indicate the RUNX1-RUNX1T1 samples. RPKM, reads per kilobase million. (*C*) Isoform-specific PCR identifies differential levels of *OGG1* mRNA nuclear isoform 1A in cell lines and patients with RUNX1-RUNX1T1 [*t* (8, 21)]. mRNA from patient samples (control samples from selected non-RUNX1-RUNX1T1 and all RUNX1-RUNX1T1) derived from the Beat AML cohort were converted to cDNA and analyzed using isoform-specific PCR primers. (*Left*) Primer design specific to isoform 1A using a primer that spans the exon 6/7 boundary unique to isoform 1A. (*Center* and *Right*) Primer design amplified between exons 6 and 7, producing a shorter product (fully spliced intron) for isoform 1A and a larger product (portion of intron retained) for isoform 1B. Isoform sequences and expected sizes of product were determined using *OGG1* isoform sequences from NCBI RefSeq. The mean values with corresponding SDs are given; each circle corresponds to a unique patient sample. (*D*) Quantification of isoform-specific mRNAs in AML cell lines, with the primer design identical to that shown in *C*. The mean values with corresponding SEs were obtained from three independent experiments. Significance is calculated versus MOLM-14. $*P < 0.05$; $**P < 0.01$.

levels of 8-oxo-dG in genomic DNA. To test this hypothesis, we isolated nuclear proteins from OGG1-proficient MOLM-14, OGG1-reduced RUNX1-RUNX1T1 (Kasumi-1 and SKNO-1), and OGG1-mutated (KG-1) AML cells and compared the abilities of these nuclear extracts to incise synthetic oligodeoxynucleotides containing an 8-oxo-dG lesion. These in vitro assays were carried out using fluorescent-labeled oligodeoxynucleotides in which a 5′ carboxytetramethylrhodamine (TAMRA)-conjugated 17-mer containing a site-specific 8-oxo-dG lesion was annealed with a complementary strand containing Black Hole Quencher 2 (BHQ2) on its 3′ terminus (*SI Appendix*, Fig. S1*A*). The control reactions were initiated by the addition of OGG1 and monitored at 37 °C in a plate reader. OGG1-catalyzed DNA incision at the lesion site and subsequent dissociation of the TAMRA-conjugated product from the complementary strand resulted in enhancement of the fluorescent signal (*SI Appendix*, Fig. S1*B*).

When nuclear extracts were tested under identical conditions, products were also formed, with the highest level observed in the presence of nuclear proteins isolated from MOLM-14 cells (*SI Appendix*, Fig. S1*C*). The area under the curve was integrated for each reaction and relative levels of OGG1-dependent DNA incision were calculated for Kasumi-1, SKNO-1, and KG-1 cell extracts using the corresponding data for MOLM-14 as the reference (Fig. 2*A*). These analyses demonstrated that compared with MOLM-14, nuclear extracts isolated from the RUNX1-RUNX1T1 or OGG1-mutated cells were less competent in incisions of 8-oxo-dG-containing DNA; the differences in incision levels observed for SKNO-1 and KG-1 versus MOLM-14 cells were statistically significant. The result obtained for KG-1 suggested that the glycosylase activity of the thermosensitive R229Q OGG1 mutant was partially restored during isolation of nuclear extracts at the permissive 4 °C temperature, consistent with the literature (30).

In addition to measuring relative levels of OGG1 incision activity, we also used an alternative approach for further validation of reduced abilities of RUNX1-RUNX1T1 AML cells to initiate the repair of nuclear 8-oxo-dG. Specifically, we used a modified comet assay designed to detect unrepaired OGG1 substrates in genomic DNA. MOLM-14, Kasumi-1, and SKNO-1 cells were harvested, permeabilized, treated with exogenous OGG1 or left untreated (±OGG1), and processed for quantitation of comet tails (Fig. 2*B*). The KG-1 cell line, which at 37 °C is essentially a null mutant with regard to OGG1 activity, was also used (30). RUNX1-RUNX1T1 cell lines had significantly more 8-oxo-dG lesions than the OGG1-proficient cell line, with levels of OGG1-specific base damage, as measured by the percent DNA in the tail and the tail moment, comparable to those detected in the KG-1 cells (Fig. 2 *C* and *D*). These data suggest that the decreased levels of nuclear OGG1 result in a BER-deficient cellular phenotype that may underlie any potential synergism with chemotherapeutic agents.

OGG1-Deficient AML Cells Are Differentially Sensitive to Ara-C Treatment but Not to General Replication Stressors. To determine whether decreased expression of nuclear *OGG1* translated to a functional loss of OGG1, cell viability was measured following exposure to either Ara-C or daunorubicin (Fig. 3 *A* and *B*). OGG1-mutated KG-1 cells were highly sensitive to Ara-C, while Kasumi-1 and SKNO-1 cells had an intermediate sensitivity and MOLM-14 cells were highly resistant, suggesting possible OGG1-dependent sensitivity (Fig. 3*A*). In contrast, treatment with increasing concentrations of daunorubicin showed no correlation between OGG1 level and survival (Fig. 3*B*).

Given the apparent OGG1-dependent sensitivity to Ara-C, we investigated whether this response was Ara-C-specific or a generalized response to replication stress. Two different known replication stressors, hydroxyurea (Fig. 3*C*) and aphidicolin (Fig. 3*D*), were used. Similar to the results of daunorubicin treatment, neither compound showed an OGG1-dependent cytotoxicity response. To further explore the specificity of the Ara-C–mediated, OGG1-dependent cytotoxicity, we tested whether a related arabinose-based replication inhibitor, Ara-G, would yield comparable survivals. This nucleoside contains the same modified sugar as Ara-C but has a guanine instead of a cytosine base (Fig. 3*G*). These data show that Ara-G did not enhance cytotoxicity in OGG1-deficient cells, indicating that the observed response to Ara-C was not indicative of a more generalized inability to cope with arabinose-based nucleoside analogs (Fig. 3*E*). We also tested whether another cytosine-based nucleoside analog, gemcitabine (Fig. 3*G*), would confer toxicity comparable to those of Ara-C; however, substitution of the arabinose sugar with difluororibose did not show any evidence of OGG1-dependent sensitivity (Fig. 3*F*).

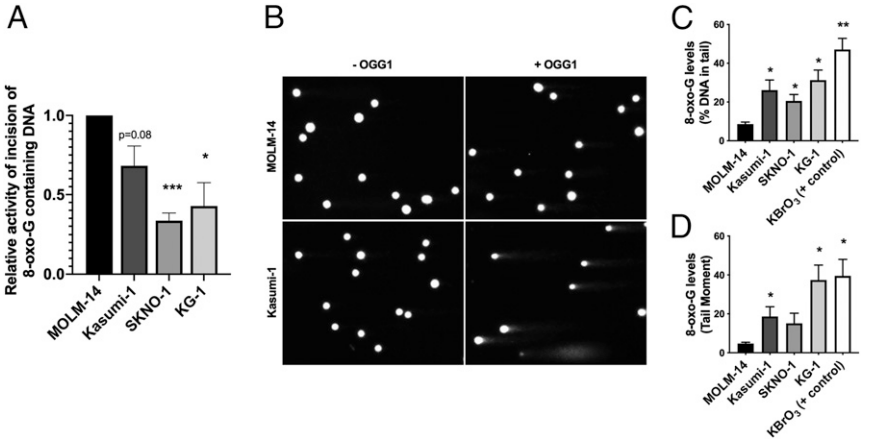

Fig. 2. Differential OGG1 activity and 8-oxoG levels in AML cells. (*A*) Relative incision activity in nuclear extracts from AML cell lines on 8-oxo-dG–containing DNAs. The mean relative activities with corresponding SEs were calculated from four independent nuclear extract preparations. (*B*) Representative images of the modified comet ± OGG1 enzyme incubation. (*C* and *D*) Percent DNA in the tail (*C*) and tail moment (*D*) to quantify differences in the modified comet assay. Values are normalized to the control (-OGG1) for each condition. For each, 100 cells were scored, and each condition was tested in biological triplicate. The mean values with corresponding SEs were obtained from three independent experiments. For all panels, significance is calculated versus OGG1-proficient MOLM-14. $*P < 0.05$; $**P < 0.01$; $***P < 0.001$.

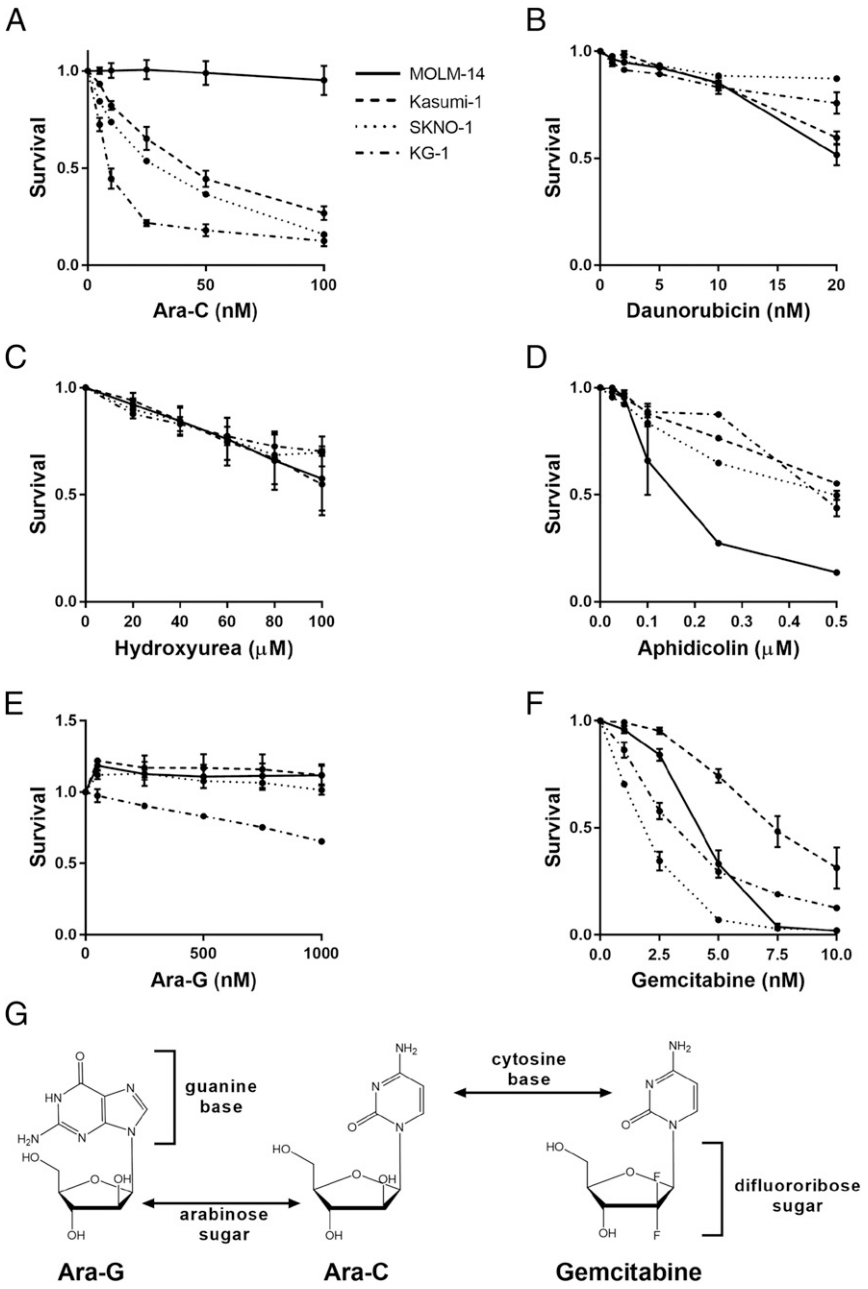

Fig. 3. OGG1-deficient AML cells are uniquely sensitive to Ara-C. AML cell lines were treated with increasing concentrations of each drug for 5 d, and survival was measured using the AlamarBlue cell viability assay. (*A*) Ara-C; (*B*) daunorubicin; (*C*) hydroxyurea; (*D*) aphidicolin; (*E*) Ara-G; (*F*) gemcitabine. For all survival assays, experiments were performed in biological triplicate, and values are mean with SE. (*G*) The structures of Ara-G, Ara-C, and gemcitabine.

Collectively, these data demonstrate a specific effect of Ara-C in OGG1-deficient cells that cannot be attributed to a general inability to cope with replication stress, or even highly similar molecules such as Ara-G or gemcitabine. These data also suggest that the observed cytotoxicity was not simply the result of impaired replication due to Ara-C incorporation, but rather to the specific combination of Ara-C and elevated levels of 8-oxo-dG damage.

Ara-C Induces Fragile Site Expression in an OGG1-dependent Manner. Since the mechanism of action of Ara-C has been primarily associated with DNA fragmentation and chain termination (31), we examined chromosome instability following treatment. As shown in Fig. 4*A*, modest levels of breaks were observed in the SKNO-1 and KG-1 cells as early as 24 h after Ara-C treatment compared to the MOLM-14 cells. All the OGG1-deficient AML cells had significantly elevated levels of chromosomal breaks after 48 h and 72 h. There were no statistical differences in the number of breaks observed among any of the OGG1-deficient cell lines at the 48 h or 72 h time points (Fig. 4*A*). Interestingly, these breaks did not follow the traditional chromosomal breakage pattern typified by homologous recombination-deficient cells (i.e., BRCA or Fanconi anemia) in response to DNA cross-linking agents, with notably low levels of radial formation given the large numbers of breaks observed (Fig. 4*B*). Ara-C–induced breaks were mapped using G-banding, and the data revealed that the sites of breakage were not random but were correlated with common fragile sites (Fig. 4*C*). Of the 450 breaks scored, 72% mapped to 5 of the 86 known common fragile sites, with the most

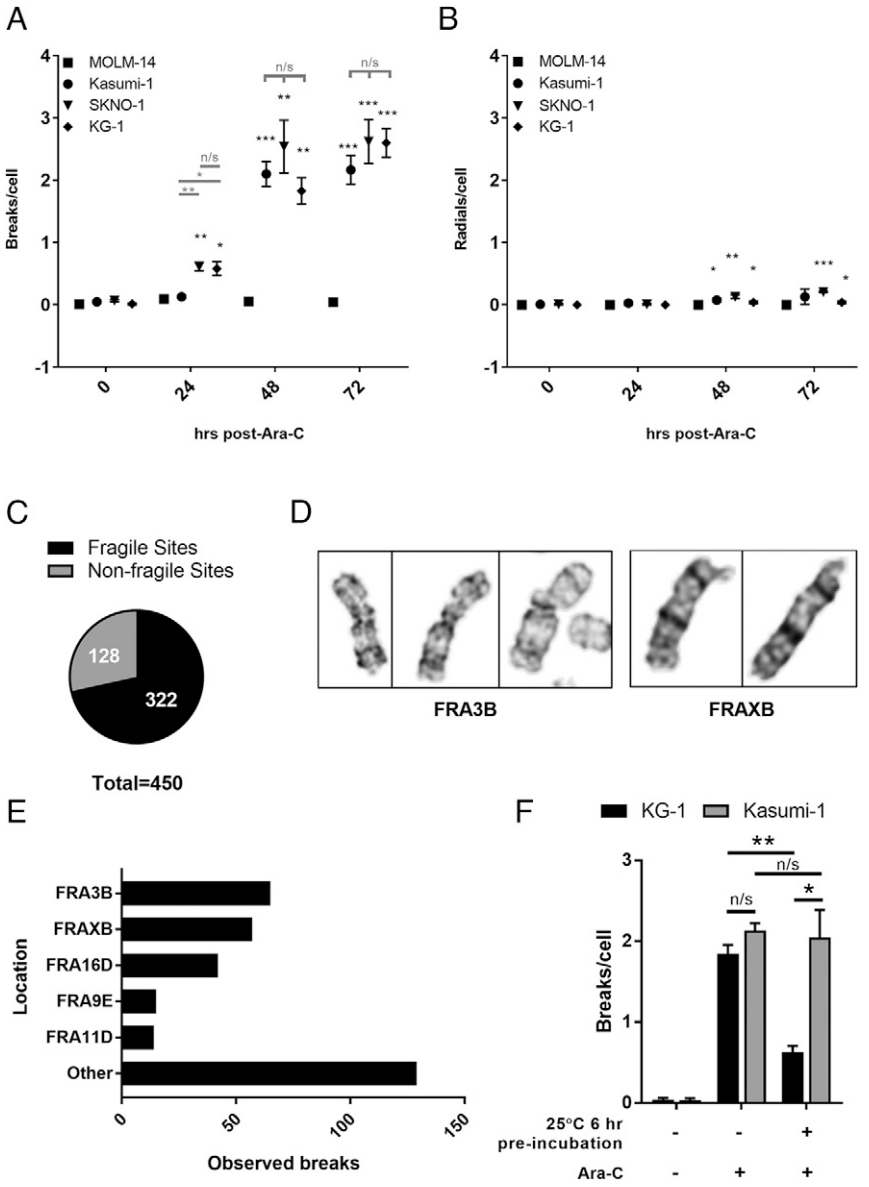

Fig. 4. Cytarabine induces fragile site breakage in OGG1-deficient cells. (*A* and *B*) Cells were treated with 100 nM Ara-C and evaluated every 24 h for signs of replication stress-induced chromatid breaks and chromosome radial formation. A time-dependent and OGG1-dependent increase in chromatid breaks was observed (*A*), but relatively few radials were detected (*B*). Experiments were performed in biological triplicate, and for each time point, 50 random metaphase cells were scored for the number of breaks and radials. Black asterisks indicate significance versus the OGG1-proficient MOLM-14 cell line at the same time point. Gray asterisks indicate differences between cell lines at a given time point. (*C*) Kasumi-1 cells were treated with 100 nM Ara-C for 48 h before harvest. Band breaks were called according to standard ISCN nomenclature using 400-band resolution. The cytogenetic locations of common fragile sites have been summarized previously (48). One hundred and fifty breaks from three independent experiments, for a total of 450 breaks, were analyzed. Graph represents the total number of breaks represented by fragile sites and nonfragile sites out of 450 analyzed. $\chi^2 = 665.32$; $P < 0.0001$. (*D*) Examples of recurrent breaks at FRA3B (3p14) and FRAXB (Xp22.3) in response to Ara-C treatment. (*E*) Five of 86 fragile sites account for 60% of the observed fragile sites in response to Ara-C. "Other" represents 56 combined fragile sites with between one and seven observed breaks each. Twenty-five common fragile sites had no observed breaks. (*F*) Eliminating 8-oxo-G lesions from DNA before Ara-C treatment reduces fragile site breaks in response to Ara-C. KG-1 cells contain a temperature-sensitive mutation (R229Q-tsOGG1) previously characterized as active at 25 °C and inactive at 37 °C. Incubation for 6 h at 25 °C allows for tsOGG1 to clear 8-oxo-dG lesions from genome down to wild-type levels. After 6 h, at 25 °C, KG-1 cells were treated with Ara-C and immediately returned to 37 °C, inactivating tsOGG1. Kasumi-1 cells were processed in parallel as a positive control for OGG1 deficiency and to ensure that appropriate replicative timing was maintained after temperature changes for the analysis of chromosome breaks. For each, 50 metaphases were analyzed, and the mean values with corresponding SEs were calculated from three independent experiments. For all panels, $*P \leq 0.05$; $**P \leq 0.01$; $***P \leq 0.001$.

prevalent being FRA3B (3p14.2; 20%), FRAXB (Xp22; 18%), and FRA16D (16q23; 13%) (Fig. 4 *D* and *E*). Although these are common fragile sites, this percentage far exceeds the expected frequency calculated for random occurrence at any fragile site (19% for all 86 fragile sites combined given 450 breaks analyzed). These common fragile sites are chromosomal locations that commonly break when cells are stressed with aphidicolin or other replication stressors and are thought to be due to a combination of factors, including delayed and prolonged replication, a paucity of origins, AT-rich sequences, and secondary DNA structures. These

data suggest that there is no Ara-C–dependent bias of fragile site expression toward any unique specific regions, but rather exacerbation of chromosomal fragility associated with generally difficult-to-replicate regions of the genome.

To move from correlation to causation, we used the KG-1 cells to switch OGG1 on and off by changing the temperature conditions before treatment with Ara-C. Prior characterization of the KG-1 cells had determined that a 6-h incubation at 25 °C was sufficient time for restoration of OGG1 activity and repair of accumulated 8-oxo-dG lesions to wild-type levels (30). To test whether elevated 8-oxo-dG levels were directly related to the observed Ara-C–dependent chromosome breaks, KG-1 and Kasumi-1 cells were incubated at 25 °C for 6 h, then treated with Ara-C and switched back to 37 °C for 48 h. The Kasumi-1 cells were used as a positive control for temperature-insensitive breaks and for any effects of the temperature shift on the breakage assay results. As shown in Fig. 4*F*, when pretreated for 6 h at 25 °C to allow sufficient time for the KG-1 cells to clear 8-oxo-dG lesions, KG-1 cells had significantly fewer breaks than Kasumi-1 cells, with a 66% reduction in breaks relative to those with no preincubation. These data demonstrate that the repair of 8-oxo-dG lesions before treatment with Ara-C directly resulted in fewer chromosomal breaks, suggesting that the sensitivity to Ara-C in OGG1-deficient cells is due to an increased burden of 8-oxo-dG lesions. Based on these data, we hypothesized that Ara-C or its metabolite must be directly interacting with 8-oxo-dG to produce the observed synergism between OGG1 deficiency and Ara-C.

Replicative DNA Polymerase δ Can Insert Ara-CMP Opposite 8-oxo-dG but Cannot Carry Out Further Extension. Considering the data presented above, it was important to elucidate molecular interactions between Ara-C and 8-oxo-dG. Thus, in vitro replication assays were conducted to determine whether the Ara-C opposite 8-oxo-dG pair can be formed and how it is different from the Ara-C opposite dG or dC opposite 8-oxo-dG pairs. Several DNA polymerases have been previously identified that are capable of Ara-C insertion opposite dG and can continue polymerization beyond that site with various degrees of efficacy (32, 33). This includes one of the two major eukaryotic DNA polymerases, polymerase (pol) ε (33). It is also known that several DNA polymerases can replicate past 8-oxo-dG by preferentially inserting a dC or dA opposite the lesion, with the efficiencies of further primer extension minimally compromised (34–41). However, the ability of DNA polymerases to insert Ara-C opposite 8-oxo-dG and extend from such a noncanonical pair has not been previously addressed. Our experimental design used pol δ, which is largely responsible for synthesis of the lagging strand, contributes to initiation of replication of the leading strand, and is a component of various DNA repair pathways (42, 43). Additionally, relative to pol ε, pol δ appears to be more tolerant to the presence of lesions on template DNA and is only moderately affected by the 8-oxo-dG lesion (35, 38–40).

DNA templates were prepared to contain an internal 8-oxo-dG or control dG at the corresponding position and annealed with a 20-mer primer designed to place the 3′ terminus immediately upstream of the target site (−1 primer) (Fig. 5*A*). Primer extension reactions were conducted in the presence of dCTP or Ara-CTP to generate the 21-mer insertion products. Subsets of the reactions were also supplemented with dGTP, which in the given sequence context would produce the 22- and 23-mer products. To evaluate activity of pol δ on an 8-oxo-dG–containing template in the presence of Ara-C, reactions were conducted with the exonuclease-proficient form of enzyme (Fig. 5 *B* and *C* and *SI Appendix*, Fig. S2*A*). The data showed that on nondamaged dG template, substitution of dCTP by Ara-CTP had no significant effect on DNA synthesis, with the incorporation of Ara-C resulting in a slight shift in electrophoretic mobility of the product bands relative to reactions containing dCTP. The relative amounts of 21-mer insertion products were indistinguishable (lanes 2 and 4). In reactions containing Ara-CTP and dGTP, very minor pausing was observed opposite dC (lane 5), with the major extension products being 23-mers, suggesting incorporation of Ara-C at both position 21 and position 23. The total amount of products beyond the target site was slightly higher in the presence of dCTP than in the presence of Ara-CTP (lanes 3 and 5), but the difference was not statistically significant. Consistent with previous analyses (40), exonuclease-proficient pol δ was also able to insert dC opposite 8-oxo-dG (lane 7) and in the presence of dGTP, extended this primer to position 23 (lane 8). In contrast, there was a significant decrease in the accumulation of insertion products on the 8-oxo-dG–containing template in the presence of Ara-CTP

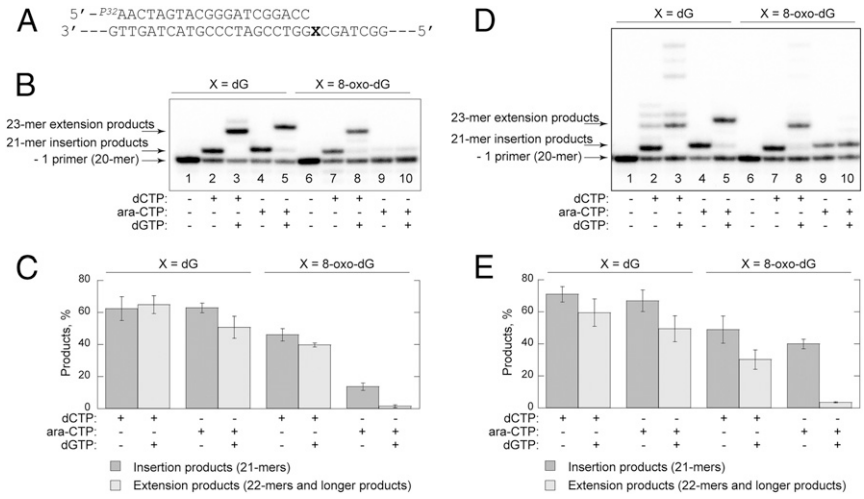

Fig. 5. Replication of DNA containing 8-oxo-dG by exonuclease-proficient and -deficient pol δ in the presence of Ara-CTP. (*A*) Structures of the −1 primer/template substrates. (*B*) Representative gel image of AraC incorporation and subsequent extension by exonuclease-proficient pol δ. Reactions were carried out for 30 min at 37 °C in the presence of 5 nM DNA substrate, 2 nM pol δ, and 100 μM dCTP or Ara-dCTP, without or with 100 μM dGTP. (*C*) Mean percentage of products with corresponding SDs that were calculated from three independent experiments using exonuclease-proficient pol δ. (*D*) Representative gel image of Ara-C incorporation and subsequent extension by exonuclease-deficient pol δ. Reactions were carried out using conditions described for *B*. (*E*) The mean percentage of products with corresponding SDs that were calculated from three independent experiments using exonuclease-deficient pol δ.

(lane 9), such that relative to the reaction supplemented with dCTP (lane 7), the amount of this product was reduced by ~3.4-fold ($P < 0.001$). Additionally, the products beyond the 8-oxo-dG site were barely detectable (lane 10). The latter result suggests that following incorporation of Ara-C opposite 8-oxo-dG, either further primer extension was strongly inhibited or nascent Ara-C could be subjected to exonucleolytic removal by pol δ.

Further investigations examined whether the presence of Ara-C opposite template dG or 8-oxo-dG would affect the exonuclease function of pol δ. The polymerase was incubated with various primer-template combinations in the absence of dNTPs (*SI Appendix*, Fig. S3). These data revealed that the exonuclease processing of a 3′-Ara-C nucleotide was considerably slower than that observed for the control 3′-dC.

To gain additional insights into the incorporation and extension properties of pol δ when synthesizing past 8-oxo-dG sites, we also examined the exonuclease-deficient form of pol δ (D520V) (Fig. 5 *D* and *E* and *SI Appendix*, Fig. S2*B*). The patterns of product formation using nondamaged template with either dCTP (lanes 2 and 3) or Ara-C (lanes 4 and 5) or using 8-oxo-dG template with dCTP (lanes 7 and 8) were very similar to the pattern observed for its exonuclease-proficient counterpart (Fig. 5 *B* and *C*). The level of incorporation of Ara-C opposite the 8-oxo-dG by exonuclease-deficient pol δ was relatively high. The amount of product was only slightly lower in the presence of Ara-CTP (lane 9) than in the presence of dCTP (lane 7), and the difference was not statistically significant. However, the extension step of reaction was strongly inhibited (lane 10). Collectively, these data reveal that pol δ can insert Ara-C opposite 8-oxo-dG, generating a replication intermediate that is inhibitory to both forward (polymerase) and reverse (exonuclease) reactions.

Discussion

The overall responsiveness of the aggregate of AML patients treated by 7+3 therapy varies widely, with patients with the two subtypes RUNX1-RUNX1T1 and CBFB-MYH11 having significantly more favorable long-term prognoses. We hypothesized that analyses of differential gene expression in favorably-responding patient subtypes may hold the key to the design of therapies for poor responders. Thus, when AML survivorship is considered without regard to specific subtype, it could be categorized as a cancer in which there are exceptional responders. In this regard, the National Cancer Institute has initiated a systematic platform and experimental strategy for studying patients who exhibit exceptional responses as part of early-phase clinical trials: the Exceptional Responders Initiative (ERI). The rationale and goals of the ERI are to gain insight into the molecular bases of these complete or partial responses, through which these data are anticipated to not only reveal the molecular features that provide predictive value for malignant tissue responses, but also to identify response-limiting pathways. Although AML responsiveness to standard of care chemotherapeutics is not specifically categorized within the ERI criteria, there are parallel concepts that could provide insight into novel approaches to identifying potential new targets for therapeutic intervention. Specifically, although prior studies have anticipated a role of OGG1 status as a potential predictor of therapeutic responsiveness (18), there have been no studies aimed at understanding the mechanistic principles to rationalize deficiencies in OGG1 levels and therapeutic responsiveness to 7+3 treatment. Furthermore, these previous studies did not make the case for a unique role for OGG1 or for OGG1 as a therapeutic target.

To justify such an assertion, it was necessary to first establish whether the low expression of *OGG1* in RUNX1-RUNX1T1 patients was a unique signature or whether other genes that function in controlling genome stability were also selectively expressed in this AML subtype. To address this issue, our investigation analyzed gene expression profiles for those genes that are consistently dysregulated in the excellent responders compared with poor responders. Of the >400 genes analyzed, *OGG1* was the only gene that appears to have low levels of expression that correlated with the good prognosis AML subtypes. Additionally, this correlation appears to affect only the nuclear splice variant (Fig. 1 *C* and *D*), a result consistent with the primary role of OGG1 in cleansing the nuclear genome of 8-oxo-dG damage. It is worth noting that in addition to AraC-induced genotoxicity via its effects on replication of nuclear DNA, AraC has also been implicated in exerting mitochondrial-associated cellular toxicities in postmitotic neurons (44). Although these studies are highly relevant to nondividing cells, we consider that the primary role of Ara-C in our studies is exerted in the nucleus, since our investigation used proliferating cultures as opposed to postmitotic neurons. Additionally, we have shown that the levels of mitochondrial-targeted OGG1 mRNA were not different in RUNX1-RUNX1T1 cells compared with other AML subtypes, suggesting that Ara-C toxicity associated with mitochondrial functions would not differ significantly between these cells. Thus, we believe that the full range of effects that we measured are localized to the nuclear compartment.

Consistent with this finding, AML cells that are deficient in OGG1 accumulate increased levels of oxidatively-induced base damage even in the absence of exogenous stressors (Fig. 2). Based on this relationship, we tested whether this decreased expression correlated with functional biological endpoints relative to the standard of care chemotherapeutic drug, Ara-C. As shown in Figs. 3*A* and 4, we observed correlations between increased cytotoxicity and chromosomal breaks induced by Ara-C treatment. Furthermore, use of the tsOGG1 KG-1 cells was particularly instructive in establishing OGG1 as the critical DNA repair enzyme associated with resistance to Ara-C treatment. Specifically, our analyses demonstrated that KG-1 cells at a nonpermissive temperature (37 °C) showed significant increases in chromosomal breaks (Fig. 4*F*) relative to permissive growth conditions (25 °C). At nonpermissive temperatures, KG-1 cells also showed high levels of endogenous oxidatively-induced DNA damage (Fig. 2 *B* and *C*). Although these data correlating OGG1 deficiency with sensitivity to Ara-C suggested that other replication-blocking agents might exert comparable cytotoxic effects in RUNX1-RUNX1T1 cells, our data revealed no differential enhanced sensitivity in OGG1-deficient versus -proficient cells to hydroxyurea (Fig. 3*C*), aphidicolin (Fig. 3*D*), Ara-G (Fig. 3*E*), or gemcitabine (Fig. 3*F*).

These data suggest a model for cell death that is dependent on elevated 8-oxo-dG in DNA and incorporation of Ara-C opposite this lesion. Using in vitro polymerase reactions, we demonstrated that formation of pairs between Ara-C and 8-oxo-dG is possible, even by action of a high-fidelity DNA polymerase (Fig. 5). We hypothesize that a subset of low-fidelity DNA polymerases which are specialized in translesion synthesis also would be able to insert Ara-C opposite 8-oxo-dG and likely continue polymerization beyond that site. Formation of such a noncanonical pair would be expected to have a severe impact on genomic integrity. It was apparent that the structure of this pair at the primer terminus differed from either Ara-C opposite dG or dC opposite 8-oxo-dG. In both of those cases, subsequent extension by pol δ was minimally affected. In contrast, incorporation of Ara-C opposite 8-oxo-dG essentially prohibited the forward and reverse reactions. We further hypothesize that the presence of Ara-C opposite 8-oxo-dG in genomic DNA would perturb the biochemistry of DNA repair, recombination, and modification, which would translate into reduced rates of replication, induced DNA strand breaks, and DNA fragmentation.

Collectively, our data provide a solid foundation for validating OGG1 as a target in AML therapeutics for patients with subtypes with normal or elevated OGG1 levels. It would be

anticipated that concomitant administration of Ara-C with OGG1 inhibitors could significantly improve the overall survival of non–RUNX1-RUNX1T1 patients.

Materials and Methods

Description of Patient Samples. Deidentified patient samples were provided by Jeffrey Tyner, OHSU, from the collection of the Beat AML cohort (28). All patients provided informed consent to participate in this study on Institutional Review Board-approved protocols, as described previously (28). The 30 RNA samples included in our study represented 26 patients, 11 with the RUNX1-RUNX1T1 translocation and 15 with other AML subtypes (two patients with serial samples). The details of each sample are presented in the *SI Appendix*, Table S2. Samples from the same patient are identified by color coding in the table.

Cell Lines. The human leukemia cell lines MOLM-14 (OGG1 proficient), Kasumi-1 and SKNO-1 (both RUNX1-RUNX1T1 fusion; OGG1 reduced), and KG-1 (tsOGG1) were kindly provided by Jeffrey Tyner, OHSU. All cells were grown and maintained in RPMI-1640 (HyClone) with 1% antibiotic-antimycotic (Gibco). MOLM-14 and KG-1 cells were supplemented with 10% FBS, Kasumi-1 cells were supplemented with 20% FBS, and SKNO-1 cells were supplemented with 15% FBS and human granulocyte macrophage colony-stimulating factor (Peprotech) at a final concentration of 10 ng/mL Cells were maintained in T25 flasks (VWR) in a humidified ambient oxygen incubator at 37 °C with 5% CO_2. All cell lines routinely tested negative for the presence of mycoplasma using the MycoAlert *Mycoplasma* Detection Kit (Lonza). Cell lines were authenticated in our laboratory via karyotyping. All cell suspensions were renewed after ∼3 mo to avoid genetic drift.

Measurement of OGG1 Transcript Levels in Patient Samples and Cell Lines. RNA that had been previously isolated from patient samples collected through the OHSU Beat AML project were diluted to <100 ng/μL prior to cDNA production. Cells from culture were collected by centrifugation for 5 min at 180 × *g*, washed in cold PBS, and recentrifuged before being flash frozen at −80 °C. RNA isolation was performed using the Direct-zol RNA MiniPrep Plus Kit (Zymo Research). cDNA was constructed from both patient RNA samples and cell line RNA using the iScript cDNA Synthesis Kit (Bio-Rad). PCR was performed using normalized cDNA concentrations (NanoDrop), DreamTaq Master Mix (Thermo Fisher Scientific), and the following primers. The forward primer for isoform 1 (5′-GACTACAGCTGGCACCCTACCAC-3′) is based in exon 6 and was used to anchor all *OGG1*-specific PCR amplifications. To amplify *OGG1* isoform 1A, a reverse primer (5′-GCACTGAACAGCACCGCTTGG-3′) was constructed that spanned the junction between *OGG1* exons 6 and 7. This 131-bp PCR product is referred to as the isoform 1A-specific product. Another reverse primer (5′-GCAGGTCGGCACTGAACAGC-3′) was based in exon 7 and when used with the forward primer generated two PCR products, 139 bp (isoform 1A) and 383 bp (isoform 1B). The PCR primers for the *GAPDH* controls used in all reactions were 5′-GTCAAGCTCATTTCCTGGTAT-3′ (forward) and 5′-CTCTCTTCCTCTTGTGCTCTTC-3′ (reverse).

The PCR conditions were T_m = 59 °C and a 30-s extension for OGG1 primers and T_m = 53 °C and a 30-s extension for GAPDH primers, for a total of 30 cycles. Reactions were performed in triplicate, and samples were run on a 5% polyacrylamide gel in 0.5% TBE for 3 h at 120 V and then stained for 1 h in GelRed. All patient samples were processed in parallel and randomized on the PCR block. To negate gel-to-gel variation in staining intensity, samples were randomized on the gels. PCR products were visualized with the FluorChem M system (Protein Simple). Analysis of band intensity was performed using ImageJ (45), and all measurements were normalized to respective GAPDH intensity.

Cytotoxicity Induced by DNA Replication Blocking Agents. For all drug treatments, cells were seeded in 96-well plates at 10,000 cells per well in technical triplicate for each drug dose. Increasing amounts of Ara-C (Tocris Biosciences), daunorubicin (Fisher Scientific), hydroxyurea (Sigma-Aldrich), aphidicolin (Sigma-Aldrich), Ara-G (Fisher Scientific), or gemcitabine (VWR) were added to cells for a total of 5 d. On day 5, cell survival was analyzed using AlamarBlue (Bio-Rad) and a TECAN plate reader. The data were plotted using Graph Pad Prism software.

Preparation of Nuclear Extracts. For preparation of nuclear extracts, cells were grown to a density of ∼2 to 4 × 10^5 cells/mL, collected by centrifugation at 180 × *g*, and fractioned using an Abcam kit (ab113474). The nuclear proteins were obtained by incubation of nuclei with Abcam extraction buffer (5 μL per 10^6 cells), followed by centrifugation at 12,000 × *g* for 10 min. The supernatant fraction was collected, kept on ice, and used in the OGG1 activity assays within 2 to 20 h. The protein concentrations were measured using Bradford reagent (Bio-Rad) and a TECAN plate reader.

DNA substrate for the OGG1 activity assays was a 17-mer double-stranded oligodeoxynucleotide containing a site-specific 8-oxo-dG, the TAMRA moiety on the 5′ terminus of the lesion-containing strand, and BHQ2 on the 3′ terminus of the complement strand (5′-TAMRA-TCACC(8-oxo-dG)TCGTACGACTC-3′ annealed with 5′-GAGTCGTACGACGGTGA-BHQ2-3′) (*SI Appendix*, Fig. S1*A*). DNA substrate preparation and the experimental approach for measurement of OGG1 activity using TAMRA-conjugated oligodeoxynucleotides have been described in detail previously (46).

To monitor incision of 8-oxo-dG-containing DNA in the presence of nuclear extracts, the DNA substrate was aliquoted into wells of a black 384-well plate, reactions were initiated by the addition of nuclear extract proteins, and the TAMRA fluorescent signal was recorded in a TECAN plate reader at 37 °C for 2 h using a 525/9-nm excitation filter and a 598/20-nm emission filter. The reactions were conducted in 20 mM Tris·HCl pH 7.4, 100 mM KCl, and 0.01% (vol/vol) Tween 20 with 50 or 250 nM DNA substrate and 0.1 or 0.2 μg/μL nuclear proteins. The reaction volume was 20 μL. Each experiment included the positive control reaction with 50 nM OGG1 to ensure that the amount of DNA substrate did not limit the product formation in reactions with nuclear proteins, as well as the negative control reaction containing Abcam extraction buffer (*SI Appendix*, Fig. S1*B*). An additional control reaction was conducted in the presence of 50 nM NEIL1 to incise DNA that contained an unidentified lesion that was a substrate for NEIL1 but not for OGG1. The fraction of this contaminating species constituted ∼5% of total DNA and was regarded as background. The data were collected from at least four independent protein extract preparations and treated as follows. The area under the curve was calculated for each reaction, and following subtraction of the corresponding value from the parallel NEIL1 reaction, relative activities of Kasumi-1, SKNO-1, and KG-1 extracts were calculated using the activity of MOLM-14 extract measured in the same experiment as a reference. The area under curve values, average relative activities with corresponding SEs, and *P* values were calculated using KaleidaGraph software (Synergy Software).

Comet Assay. A modified comet assay was performed with the OGG1-FLARE kit (Trevigen) with modifications. The positive control was a 3-h treatment with 200 μM $KBrO_3$. Cells were collected by centrifugation at 180 × *g* for 5 min and resuspended in serum-free medium at a density of 10^5/mL, followed by gentle mixing in a 1:2 ratio with 37 °C low-melting agar. The suspension was quickly pipetted onto 37 °C FLARE slides. Once a ring of dried agar appeared around the edge of each well, parafilm was placed over the slide, and agar was set at 4 °C for 45 min. Parafilm was gently removed prior to incubation in chilled lysis buffer overnight. Slides were processed according to the supplier's instructions. In brief, slides were soaked in FLARE buffer and then incubated in either buffer alone (−OGG1) or buffer with OGG1 enzyme (+OGG1) under a parafilm coverslip at 37 °C in a preequilibrated humid chamber. Parafilm was then removed, and slides were soaked in alkaline electrophoresis buffer prior to running at 24 V for 30 min. Samples were neutralized in 0.4 M Tris·HCl, dried, and stained with SYBR Gold for 30 min at room temperature. Slides were imaged at 10× magnification with a Keyence BZ-X710 microscope. Each condition was tested in biological triplicate. For each well, 100 cells were scored using CometScore v1.5.

Chromosomal Breakage Assay. Cells were plated at 8 × 10^5 cells/mL in a 6-well plate and treated with agents for indicated times. The cells were harvested by centrifugation at 180 × *g* for 5 min and the pellet was resuspended in warmed hypotonic solution (75 mM KCl, 5% FBS) for 10 min. A 3:1 methanol:acetic acid fixative was added to each tube, and the cell pellet was collected and resuspended in 3 mL of the fixative at room temperature for 15 min. The cells were pelleted and then stored at −20 °C until being dropped and stained for chromosomal breakage analyses.

Chromosome Fragile Site Analyses. Kasumi-1 cells were treated with 100 nM Ara-C for 48 h prior to harvest. Colcemid (0.05 μg/mL) was added for 3 h to arrest cells at metaphase. Cells were harvested as described above, fixed on slides, and baked at 90 °C for 20 min. After cooling, cells were trypsinized for 45 s, stained with Wright's stain for 80 s, rinsed with H_2O, and dried. Chromosome breaks were imaged using bright field microscopy at 100× magnification and analyzed using CytoVision software (Applied Imaging). Breakpoints were identified according to standard ISCN nomenclature (47) using 400-band resolution. The cytogenetic locations of common fragile sites have been reported previously (48). A total of 150 breaks were scored in each of three independent experiments, for a total of 450 breaks per data point.

Preparation of DNA Substrates for In Vitro Replication Assays. All unmodified oligodeoxynucleotides, a 12-mer oligodeoxynucleotide containing an internal 8-oxo-dG, and a 21-mer oligodeoxynucleotide containing 3′-terminal Ara-C were synthesized and purified by Integrated DNA Technologies. The 59-mer oligodeoxynucleotides used as templates for in vitro polymerase reactions were constructed according to a published procedure (40) and were described previously (49). The sequence of templates was 5′-ACGGCCAGTGAGGCTAGCXGGTCCGATCCCGTACTAGTTGCTTCCTGCAGGCGTAATCA-3′, where X was either dG or 8-oxo-dG. The sequences of oligodeoxynucleotides used as primers were as follows: 5′-AACTAGTACGGGATCGGACC-3′ (-1 primer), 5′-ACTAGTACGGGATCGGACCC-3′ (0-dC primer), and 5′-ACTAGTACGGGATCGGACC (Ara-C)-3′ (0-Ara-C primer). Primer oligodeoxynucleotides were radioactively labeled with ^{32}P-γ-ATP using T4 polynucleotide kinase (New England BioLabs) and annealed to templates as described previously (49).

Replication Assays In Vitro. Ara-C triphosphate (Ara-CTP) was purchased from Abcam (ab146731). Recombinant *Saccharomyces cerevisiae* pol δ (Pol3-Pol31-Pol32) and its exonuclease-deficient D520V variant, a generous gift from Peter Burgers, were overexpressed and isolated as reported previously (50, 51). Polymerase reactions contained 5 nM DNA substrate and were conducted at 37 °C in a buffer composed of 25 mM Tris·HCl pH 7.5, 10 mM NaCl, 8 mM Mg_2Cl, 10% glycerol, 100 μg/mL bovine serum albumin, and 5 mM dithiothreitol. Concentrations of pol δ, dNTPs, and Ara-CTP and incubation times are specified in the figures or figure legends. The substrate and product primers were resolved by electrophoresis in a 15% denaturing polyacrylamide gel containing 8 M urea in Tris-borate-EDTA buffer and visualized using a Personal Molecular Imager (Bio-Rad). The gel images were analyzed by the Personal Molecular Imager built-in software. The mean percentages of polymerization and exonucleolytic cleavage products with corresponding SDs were calculated from three independent experiments using KaleidaGraph 4.1 software (Synergy Software). The *P* values were calculated using Student's *t* test.

Statistical Methods. All experiments were repeated as specified for each dataset, and significance was calculated using either an unpaired or paired Student's *t* test, as applicable. The specific analyses are indicated with each dataset. For all experiments, *P* values are indicated as follows: $*P \leq 0.05$; $**P \leq 0.01$; $***P \leq 0.001$. For the fragile site analyses, the χ^2 test was performed to determine significance.

Data Availability. All study data are included in the main text and/or *SI Appendix*.

ACKNOWLEDGMENTS. We thank Dr. Jeffrey Tyner and members of his laboratory at OHSU for assistance in obtaining the AML mRNA samples from the Beat AML project, providing the cell lines, and providing insightful comments on the manuscript. We also thank Dr. Beth Wilmot and Dr. Shannon McWeeney for assistance with Vizome data analyses and Dr. Peter Burgers (Washington University) for the gift of the purified exonuclease-proficient and -deficient DNA polymerase δ. This work was supported by NIH Grant R21 CA216551, the OHSU Knight Cancer Institute Pilot Grant Program, and an OHSU Oregon Clinical and Translational Research Institute catalyst grant. A.K.M. and R.S.L. acknowledge support from the Oregon Institute of Occupational Health Sciences at OHSU via funds from the Division of Consumer and Business Services of the State of Oregon (ORS 656.630).

1. National Cancer Institute, Surveillance, Epidemiology, and End Results Program (SEER), Cancer stats facts: Leukemia-acute myeloid leukemia. https://seer.cancer.gov/statfacts/html/amyl.html. Accessed 1 November 2019.
2. A. R. Derolf *et al.*, Improved patient survival for acute myeloid leukemia: A population-based study of 9729 patients diagnosed in Sweden between 1973 and 2005. *Blood* **113**, 3666–3672 (2009).
3. W. Abdel-Aziz, H. Y. Jiang, R. J. Hickey, L. H. Malkas, Ara-C affects formation of cancer cell DNA synthesome replication intermediates. *Cancer Chemother. Pharmacol.* **45**, 312–319 (2000).
4. H. Y. Jiang, R. J. Hickey, W. Abdel-Aziz, L. H. Malkas, Effects of gemcitabine and araC on in vitro DNA synthesis mediated by the human breast cell DNA synthesome. *Cancer Chemother. Pharmacol.* **45**, 320–328 (2000).
5. Y. Pommier, E. Leo, H. Zhang, C. Marchand, DNA topoisomerases and their poisoning by anticancer and antibacterial drugs. *Chem. Biol.* **17**, 421–433 (2010).
6. F. L. Hogan, V. Williams, S. Knapper, FLT3 inhibition in acute myeloid leukaemia: Current knowledge and future prospects. *Curr. Cancer Drug Targets* **20**, 513–531 (2020).
7. K. Saleh, N. Khalifeh-Saleh, H. R. Kourie, Acute myeloid leukemia transformed to a targetable disease. *Future Oncol.* **16**, 961–972 (2020).
8. K. Tzogani *et al.*, European Medicines Agency review of midostaurin (Rydapt) for the treatment of adult patients with acute myeloid leukaemia and systemic mastocytosis. *ESMO Open* **4**, (2019).
9. J. S. Becker, A. T. Fathi, Targeting IDH mutations in AML: Wielding the double-edged sword of differentiation. *Curr. Cancer Drug Targets* **20**, 490–500 (2020).
10. G. J. Roboz *et al.*, Ivosidenib induces deep durable remissions in patients with newly diagnosed IDH1-mutant acute myeloid leukemia. *Blood* **135**, 463–471 (2020).
11. J. H. Choi, J. M. Bogenberger, R. Tibes, Targeting apoptosis in acute myeloid leukemia: Current status and future directions of BCL-2 inhibition with venetoclax and beyond. *Target. Oncol.* **15**, 147–162 (2020).
12. A. H. Wei *et al.*, Venetoclax plus LDAC for newly diagnosed AML ineligible for intensive chemotherapy: A phase 3 randomized placebo-controlled trial. *Blood* **135**, 2137–2145 (2020).
13. M. Byrne *et al.*, The use of venetoclax-based salvage therapy for post-hematopoietic cell transplantation relapse of acute myeloid leukemia. *Am. J. Hematol.* **95**, 1006–1014 (2020).
14. G. Castelli, E. Pelosi, U. Testa, Targeting histone methyltransferase and demethylase in acute myeloid leukemia therapy. *OncoTargets Ther.* **11**, 131–155 (2017).
15. A. V. Krivtsov *et al.*, A menin-MLL inhibitor induces specific chromatin changes and eradicates disease in models of MLL-rearranged leukemia. *Cancer Cell* **36**, 660–673.e11 (2019).
16. R. Lu, G. G. Wang, Pharmacologic targeting of chromatin modulators as therapeutics of acute myeloid leukemia. *Front. Oncol.* **7**, 241 (2017).
17. H. Döhner *et al.*, Diagnosis and management of AML in adults: 2017 ELN recommendations from an international expert panel. *Blood* **129**, 424–447 (2017).
18. K. Liddiard, R. Hills, A. K. Burnett, R. L. Darley, A. Tonks, OGG1 is a novel prognostic indicator in acute myeloid leukaemia. *Oncogene* **29**, 2005–2012 (2010).
19. M. Dizdaroglu, E. Coskun, P. Jaruga, Repair of oxidatively induced DNA damage by DNA glycosylases: Mechanisms of action, substrate specificities and excision kinetics. *Mutat. Res.* **771**, 99–127 (2017).
20. O. Krejci *et al.*, p53 signaling in response to increased DNA damage sensitizes AML1-ETO cells to stress-induced death. *Blood* **111**, 2190–2199 (2008).
21. M. Alcalay *et al.*, Acute myeloid leukemia fusion proteins deregulate genes involved in stem cell maintenance and DNA repair. *J. Clin. Invest.* **112**, 1751–1761 (2003).
22. J. W. Hyun *et al.*, Leukemic cell line, KG-1 has a functional loss of hOGG1 enzyme due to a point mutation and 8-hydroxydeoxyguanosine can kill KG-1. *Oncogene* **19**, 4476–4479 (2000).
23. J. W. Hyun *et al.*, 8-hydroxydeoxyguanosine causes death of human leukemia cells deficient in 8-oxoguanine glycosylase 1 activity by inducing apoptosis. *Mol. Cancer Res.* **1**, 290–299 (2003).
24. L. Taricani, F. Shanahan, R. H. Pierce, T. J. Guzi, D. Parry, Phenotypic enhancement of thymidylate synthetase pathway inhibitors following ablation of Neil1 DNA glycosylase/lyase. *Cell Cycle* **9**, 4876–4883 (2010).
25. J. W. Hyun *et al.*, Radiation sensitivity depends on OGG1 activity status in human leukemia cell lines. *Free Radic. Biol. Med.* **32**, 212–220 (2002).
26. T. J. Ley *et al.*; Cancer Genome Atlas Research Network, Genomic and epigenomic landscapes of adult de novo acute myeloid leukemia. *N. Engl. J. Med.* **368**, 2059–2074 (2013).
27. E. Juarez *et al.*, An RNAi screen in human cell lines reveals conserved DNA damage repair pathways that mitigate formaldehyde sensitivity. *DNA Repair (Amst.)* **72**, 1–9 (2018).
28. J. W. Tyner *et al.*, Functional genomic landscape of acute myeloid leukaemia. *Nature* **562**, 526–531 (2018).
29. A. Ogawa, T. Watanabe, S. Shoji, C. Furihata, Enzyme kinetics of an alternative splicing isoform of mitochondrial 8-oxoguanine DNA glycosylase, ogg1-1b, and compared with the nuclear ogg1-1a. *J. Biochem. Mol. Toxicol.* **29**, 49–56 (2015).
30. P. German *et al.*, Activation of cellular signaling by 8-oxoguanine DNA glycosylase-1-initiated DNA base excision repair. *DNA Repair (Amst.)* **12**, 856–863 (2013).
31. S. Grant, Modulation of ara-C induced apoptosis in leukemia by the PKC activator bryostatin 1. *Front. Biosci.* **2**, d242–d252 (1997).
32. Y. W. Chen, J. E. Cleaver, F. Hanaoka, C. F. Chang, K. M. Chou, A novel role of DNA polymerase eta in modulating cellular sensitivity to chemotherapeutic agents. *Mol. Cancer Res.* **4**, 257–265 (2006).
33. M. Tsuda *et al.*, The dominant role of proofreading exonuclease activity of replicative polymerase ε in cellular tolerance to cytarabine (Ara-C). *Oncotarget* **8**, 33457–33474 (2017).
34. L. G. Brieba *et al.*, Structural basis for the dual coding potential of 8-oxoguanosine by a high-fidelity DNA polymerase. *EMBO J.* **23**, 3452–3461 (2004).
35. H. J. Einolf, F. P. Guengerich, Fidelity of nucleotide insertion at 8-oxo-7,8-dihydroguanine by mammalian DNA polymerase delta. Steady-state and pre-steady-state kinetic analysis. *J. Biol. Chem.* **276**, 3764–3771 (2001).
36. G. W. Hsu, M. Ober, T. Carell, L. S. Beese, Error-prone replication of oxidatively damaged DNA by a high-fidelity DNA polymerase. *Nature* **431**, 217–221 (2004).
37. J. M. Krahn, W. A. Beard, H. Miller, A. P. Grollman, S. H. Wilson, Structure of DNA polymerase beta with the mutagenic DNA lesion 8-oxodeoxyguanine reveals structural insights into its coding potential. *Structure* **11**, 121–127 (2003).
38. S. D. McCulloch, R. J. Kokoska, P. Garg, P. M. Burgers, T. A. Kunkel, The efficiency and fidelity of 8-oxo-guanine bypass by DNA polymerases delta and eta. *Nucleic Acids Res.* **37**, 2830–2840 (2009).
39. X. Meng *et al.*, DNA damage alters DNA polymerase delta to a form that exhibits increased discrimination against modified template bases and mismatched primers. *Nucleic Acids Res.* **37**, 647–657 (2009).

40. I. G. Minko, C. J. Rizzo, R. S. Lloyd, Mutagenic potential of nitrogen mustard-induced formamidopyrimidine DNA adduct: Contribution of the non-canonical α-anomer. *J. Biol. Chem.* **292**, 18790–18799 (2017).
41. A. Patra *et al*., Kinetics, structure, and mechanism of 8-Oxo-7,8-dihydro-2′-deoxyguanosine bypass by human DNA polymerase η. *J. Biol. Chem.* **289**, 16867–16882 (2014).
42. M. A. Garbacz *et al*., Evidence that DNA polymerase δ contributes to initiating leading strand DNA replication in Saccharomyces cerevisiae. *Nat. Commun.* **9**, 858 (2018).
43. S. A. Lujan, J. S. Williams, T. A. Kunkel, DNA polymerases divide the labor of genome replication. *Trends Cell Biol.* **26**, 640–654 (2016).
44. M. Zhuo, M. F. Gorgun, E. W. Englander, Neurotoxicity of cytarabine (Ara-C) in dorsal root ganglion neurons originates from impediment of mtDNA synthesis and compromise of mitochondrial function. *Free Radic. Biol. Med.* **121**, 9–19 (2018).
45. C. A. Schneider, W. S. Rasband, K. W. Eliceiri, NIH image to ImageJ: 25 years of image analysis. *Nat. Methods* **9**, 671–675 (2012).
46. A. C. Jacobs *et al*., Inhibition of DNA glycosylases via small molecule purine analogs. *PLoS One* **8**, e81667 (2013).
47. L. Shaffer, M. Slovac, L. Campbell, *ISCN 2009: An International System for Human Cytogenetic Nomenclature*(Karger, 2009).
48. S. G. Durkin, T. W. Glover, Chromosome fragile sites. *Annu. Rev. Genet.* **41**, 169–192 (2007).
49. M. Kanuri *et al*., Error-prone translesion synthesis past gamma-hydroxypropano deoxyguanosine, the primary acrolein-derived adduct in mammalian cells. *J. Biol. Chem.* **277**, 18257–18265 (2002).
50. P. M. Burgers, K. J. Gerik, Structure and processivity of two forms of Saccharomyces cerevisiae DNA polymerase delta. *J. Biol. Chem.* **273**, 19756–19762 (1998).
51. J. M. Fortune, C. M. Stith, G. E. Kissling, P. M. Burgers, T. A. Kunkel, RPA and PCNA suppress formation of large deletion errors by yeast DNA polymerase delta. *Nucleic Acids Res.* **34**, 4335–4341 (2006).